Auto-Induced, Radiofrequency, Downlink Exposure Focused at the Human Ear

Hanne Herssens, Arno Thielens
Department of Information Technology, Ghent University-imec, 9000 Ghent, Belgium
hanne.herssens@ugent.be

***Abstract* — A numerical study is performed to determine the auto-induced downlink exposure due to 5G New Radio (NR) networks at 3.5 GHz. The exposure scenario consists of a subject situated in the far-field of the base station (BS) equipped with Multiple-Input-Multiple-Output (MIMO) technology and the user equipment (UE) located next to the ear with the BS using two different precoding schemes, i.e., maximum ratio transmission and equal gain transmission, emulating a call over 5G NR. The localized absorption in the head is quantified as a function of the distance between the UE and the ear using two different exposure quantities, i.e., $\mathrm{SAR_{ear}}$ and $\mathrm{psSAR_{10g}}$. Two normalization strategies of the exposure were applied, i.e., normalizing to the average incident power density in free space and normalizing to the incident power density found at the UE. Additionally, two different phantoms were used to assess the exposure and no significant differences were found.**

***Keywords* — RF-EMF exposure, 5G, FDTD.**

I. Introduction

The introduction of the 5th generation of telecommunications technologies (5G) raises public concern about human exposure to radiofrequency electromagnetic fields (RF-EMFs). The RF-EMF exposure in 5G networks differs from the RF-EMF exposure in legacy technologies (2G-4G) and therefore the RF-EMF exposure needs to be assessed differently. In legacy technologies, downlink (DL) data transmission occurs over fixed beams. Therefore, the DL exposure could be assessed by performing numerical simulations using uncorrelated or stochastically interfering plane waves, when the exposed person is situated in the far-field region of the RF system [1]. This approach cannot be used to determine the RF-EMF exposure due to 5G networks, because the base stations (BSs) in 5G networks make use of Multiple-Input-Multiple-Output (MIMO) technology [2]. These BSs are equipped with a large number of antenna elements (antenna array) that can be precoded, i.e., controlling the amplitudes and phases of the BS antennas such that their signals will combine constructively at the intended receiver (user equipment, UE) and potentially destructively at the other receivers. This leads to a narrow beam towards or an EMF hotspot at the UE, which results in a higher signal-to-noise ratio at the UE in comparison with non-precoded transmission. This precoding will constantly adapt and therefore lead to constantly changing EMFs.

The DL exposure in 5G networks highly depends on being a user or non-user, since a user will pull the beam or hotspot towards the UE. In legacy technologies, the DL exposure does not depend on being a user or non-user. This exposure is denoted auto-induced DL (a-DL) exposure in literature [3] and is the subject of this study.

The goal of this paper is to determine the a-DL exposure at $3.5\,\mathrm{GHz}$, a frequency used in the current rollout of 5G new radio (NR) networks, in terms of the localized specific absorption rate (SAR, $\mathrm{W/kg}$) when the UE is located next to the head by performing numerical simulations. Two different localized exposure quantities are assessed as a function of the distance between the UE and the ear and compared. Additionally, two different phantoms (one female and one male) are used and the results are compared. Finally, two normalization strategies of the exposure quantities are applied.

II. Methods

A. Numerical Approach

The simulations to assess the a-DL exposure are performed with the Finite-Difference Time-Domain method in Sim4Life (ZMT, Zürich, Switzerland) using the ViP Duke and Ella heterogeneous phantoms [4] with dielectric parameters found in [5]. The phantoms are discretized with a grid step of $2\,\mathrm{mm}$ in each direction. The UE is a virtual device with vertical polarization located next to the left ear. Only the phantom's head is included in the FDTD domain which is shown in Fig. 1. We assume that the base station is found in the far-field of the user and that the incident fields can come from any direction, i.e., for every ϕ and θ in Fig. 1. The incident fields are modelled as $N = 80$ plane wave sources with their wave vectors distributed uniformly over the unit sphere [6]. Since it is assumed that the UE has a vertical polarization, the plane waves are also vertically polarized (E_θ-polarization). The simulation duration per plane wave simulation is set to 15 periods.

B. Precoding Schemes

To ensure that the plane waves interfere constructively at the UE, the EMFs are precoded. The precoded electric field focused at UE k, can be written as:

$$\mathbf{E}_k^{prec}(\mathbf{r}) = \sum_{l=0}^{N-1} \alpha_k w_{kl} \mathbf{E}_l(\mathbf{r}) \tag{1}$$

with α_k a normalization constant, w_{kl} the precoding weight and $\mathbf{E}_l$ the electric field obtained with plane wave l. The normalization constant is chosen such that

$$||\alpha_k \mathbf{w}_k|| = 1, \tag{2}$$

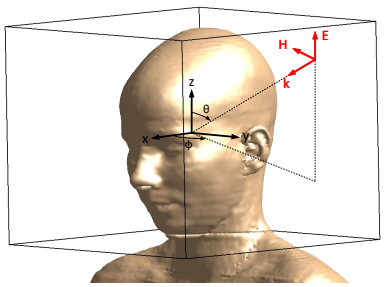

Fig. 1. The FDTD domain ($300\,\mathrm{mm} \times 300\,\mathrm{mm} \times 250\,\mathrm{mm}$) that is used for the numerical simulations is shown with an example of an incident plane wave in red. The head of the ViP Ella phantom is also shown.

with $\mathbf{w}_k = \begin{bmatrix} w_{k0} & \dots & w_{kN-1} \end{bmatrix}$.

The weights depend on the precoding technique and two different schemes are applied, i.e., maximum ratio transmission (MRT) and equal gain transmission (EGT) [7]. With MRT, the base station antennas configure both the phase and amplitude. With EGT, the base station antennas configure only the phase, while the amplitude stays constant. Therefore, when focusing at UE k:

$$w_{kl}^{MRT} = E_{z,kl}^{*} \tag{3}$$

$$w_{kl}^{EGT} = \exp\left(-j * arg(E_{z,kl})\right) \tag{4}$$

with * the complex conjugate and $E_{z,kl}$ the z-component of the electric field at UE k obtained with plane wave l.

C. Exposure Assessment

Most of the a-DL exposure will be found near the UE [6]. In this work, the UE is placed next to the left ear, therefore the organ-specific averaged SAR in the left ear ($\mathrm{SAR_{ear}}$) is used to quantify the exposure. Additionally, this exposure quantity is compared with the peak-spatial SAR averaged over 10g cube ($\mathrm{psSAR_{10g}}$), since the mass of the ear is approximately $10\,\mathrm{g}$ ($8.6\,\mathrm{g}$ and $10.6\,\mathrm{g}$ for Ella and Duke, respectively). The maximum allowed $\mathrm{psSAR_{10g}}$ is standardized by the International Commission on Non-Ionizing Radiation Protection (ICNIRP) which is set to $2\,\mathrm{W/kg}$ for the general public [8].

The incident power density ($\mathrm{S_{inc}}$) is set as a reference level at $3.5\,\mathrm{GHz}$ by the ICNIRP and the maximum allowed value is set to $10\,\mathrm{W/m^2}$ for the general public [8]. Therefore, we define β ($\mathrm{m^2/kg}$) as the exposure quantity ($\mathrm{SAR_{ear}}$ or $\mathrm{psSAR_{10g}}$) normalized to the time-average power density flux, i.e., the real part of the EM-field Poynting vector. However, these normalized exposure quantities will depend on the definition of $\mathrm{S_{inc}}$. In this paper, two different normalization strategies are investigated. In the first one, the exposure quantities are normalized to the average incident power density ($\mathrm{S_{inc,avg}}$) in the domain obtained with the plane wave sources defined in (1), when no user is present. This normalization depends on the computational domain. A bigger domain will lead to a lower $\mathrm{S_{inc,avg}}$, since the power density will be focused at the UE. In this case, we are averaging over a volume of $300 \times 300 \times 250\,\mathrm{mm^3}$. In the second strategy, the exposure quantities are normalized to the power density at the intended focus point ($\mathrm{S_{inc,focus}}$), i.e., the UE. These normalized exposure quantities scale directly with the signal strength needed by the UE. Note that the intended focus point is not necessarily the actual focus point or the location of the peak power density.

The exposure will be investigated as a function of the distance between the left ear and the focus point (y-coordinate of UE in Fig. 1). The x- and z-coordinates of the focus points are chosen such that the UE is found approximately at the location where a phone will be held in a real situation. This differs for the Duke and Ella phantom. For the Duke phantom, $x = -1\,\mathrm{mm}$ and $z = -30\,\mathrm{mm}$ is chosen. For the Ella phantom, $x = -11\,\mathrm{mm}$ and $z = -18\,\mathrm{mm}$ is chosen. The y-coordinate is varied from $y = 63\,\mathrm{mm}$ (focus point in ear) to $y = 147\,\mathrm{mm}$ (end of domain).

III. Results

A. Power Density Flux Focusing

Fig. 2 shows the time-average power density flux for the Ella phantom using MRT precoding. A strong focusing is found near the UE (red circle). However, the peak power density is found in the left ear and not at the UE. This is because the EMFs will be concentrated around the ear due to its high curvatures.

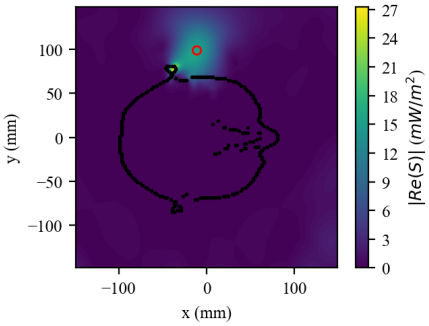

Fig. 2. The time-average power density flux focused at the UE (red circle) in the xy-plane ($z = -18\,\mathrm{mm}$) for the Ella phantom using MRT precoding with $S_{inc,avg} = 1.1\,\mathrm{mW/m^2}$.

B. Comparison Between Different Exposure Quantities

Fig. 3 shows $\mathrm{SAR_{ear}}$ and $\mathrm{psSAR_{10g}}$ as a function of the distance between the focus point and ear of the Ella phantom when MRT and EGT precoding is applied. The same behaviour is seen for $\mathrm{SAR_{ear}}$ and $\mathrm{psSAR_{10g}}$. The peak SAR will therefore be found in the ear when focusing near the ear. This was also seen in [6]. $\mathrm{SAR_{ear}}$ is higher than $\mathrm{psSAR_{10g}}$ for all distances of the focus points. The $\mathrm{psSAR_{10g}}$ contains a lot of air compared to $\mathrm{SAR_{ear}}$, since the ear has a more complex shape than a cube. Therefore, $\mathrm{psSAR_{10g}}$ is lower than $\mathrm{SAR_{ear}}$.

C. Comparison Between Different Phantoms

To see if this behavior changes for another phantom, $\mathrm{SAR_{ear}}$ as a function of the distance between the ear and focus point is also determined using the Duke phantom. Fig. 4 shows

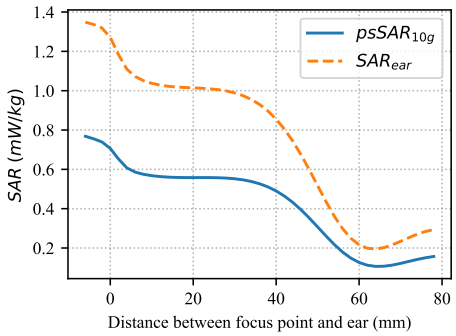

(a)

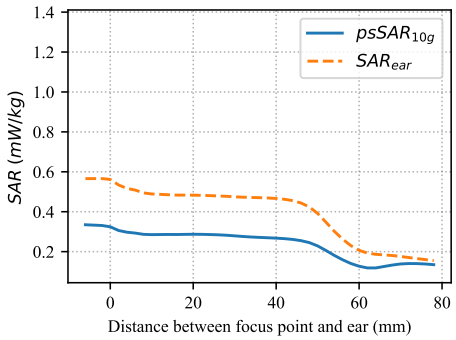

(b)

Fig. 3. Comparison of $\mathrm{SAR_{ear}}$ and $\mathrm{psSAR_{10g}}$ as a function of distance between the focus point and ear of the Ella phantom. (a) MRT, $S_{inc,avg} = 1.1\,\mathrm{mW/m^2}$. (b) EGT, $S_{inc,avg} = 0.7\,\mathrm{mW/m^2}$.

that $\mathrm{SAR_{ear}}$ determined using the Duke phantom is almost the same as when using the Ella phantom for both MRT and EGT precoding. From this, it can be concluded that the DL exposure as a function of the distance of the focus point is not phantom dependent.

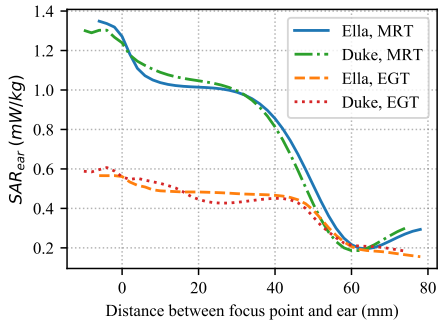

Fig. 4. Comparison of $\mathrm{SAR_{ear}}$ as a function of distance between the focus point and ear of the Ella and Duke phantom using MRT ($S_{inc,avg} = 1.1\,\mathrm{mW/m^2}$) and EGT ($S_{inc,avg} = 0.7\,\mathrm{mW/m^2}$).

D. Normalized Exposure

The normalized exposure quantities (β) as a function of distance to the focus point for the Ella and Duke phantom is shown in Fig. 5 and Fig. 6, respectively. These normalized exposure quantities are compared with $\beta_{ref} = 0.2\,\mathrm{m^2/kg}$ calculated from the basic restrictions set by ICNIRP for the general public, i.e., $\mathrm{SAR_{10g}^{ICNIRP}} = 2\,\mathrm{W/kg}$, $\mathrm{S_{inc}^{ICNIRP}} = 10\,\mathrm{W/m^2}$. If the normalized exposure is higher than β_{ref}, it means that the basic restrictions would be exceeded if $\mathrm{S_{inc}}$ is set to the reference level ($\mathrm{S_{inc}^{ICNIRP}} = 10\,\mathrm{W/m^2}$).

From these figures, it can be concluded that the normalized exposures are not phantom dependent. The normalizations as a function of distance show the same behaviour and same order of magnitude for both the Ella and Duke phantom. Normalizing the exposure quantities also results in the same order of magnitude of β for both MRT and EGT, while this was not the case when using only the normalization by (2). Fig. 3 shows that the SAR values obtained with MRT and EGT differ by a factor of 2.

The choice of exposure quantity and the definition of the incident power density determines if the limit set by ICNIRP is exceeded or not. Normalizing to $\mathrm{S_{inc,avg}}$ almost always results in exceeding the limit for both $\mathrm{SAR_{ear}}$ and $\mathrm{psSAR_{10g}}$ using both MRT and EGT precoding. Only when using $\mathrm{psSAR_{10g}}$, the limit is not exceeded for a few distances, e.g., when using the Ella phantom, the limit is not exceeded for distances between 60 and 74 mm. In contrast to this, normalizing to $\mathrm{S_{inc,focus}}$ almost always complies with the limit. The limit is exceeded for the focus points lying furthest in the ear and using $\mathrm{SAR_{ear}}$. This shows that it is important to standardize these normalizations such that the 5G exposure can be reliably compared with the basic restrictions set by ICNIRP.

The normalized exposure when using $\mathrm{S_{inc,focus}}$ (β_{focus}) is directly related to the incident power density needed by the device. If the UE needs $\mathrm{S_{inc,UE}}$ to operate, the exposure as a function of distance can be quantified by multiplying β_{focus} with $\mathrm{S_{inc,UE}}$. Fig. 5 and 6 show that for some distances the MRT precoding will lead to a lower exposure than the EGT precoding, when a certain $\mathrm{S_{inc,UE}}$ is needed. For the smaller distances, EGT will result in a lower exposure, while for the larger distances, MRT will result in a lower exposure. The distance where this transition happens is between 16 mm (0.19λ) and 24 mm (0.28λ) depending on the phantom and exposure quantity. In our future research, we will focus on how these quantities depend on the wavelength, phantom, and UE location around the phantom.

IV. Conclusion

Numerical simulations are performed to determine the localized exposure at 3.5 GHz focused at the ear for 5G networks. Two exposure quantities were assessed, i.e., $\mathrm{SAR_{ear}}$ and $\mathrm{psSAR_{10g}}$, as a function of the distance between the ear and the focus point using two different phantoms when two different precoding techniques are applied, i.e., MRT and EGT. There are no significant differences found in the exposure quantities between the two different phantoms. $\mathrm{SAR_{ear}}$ and $\mathrm{psSAR_{10g}}$ follow the same behavior as a function of distance, but $\mathrm{SAR_{ear}}$ is higher than $\mathrm{psSAR_{10g}}$. The peak SAR will therefore be found in the ear when focusing at the ear which is in agreement with literature. The normalized exposure

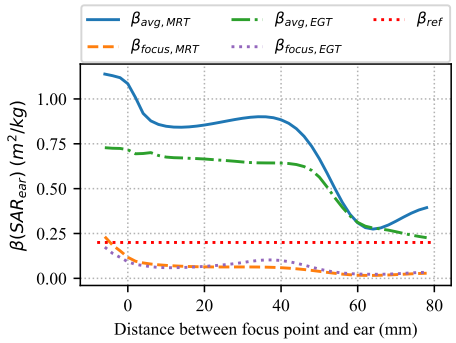

(a)

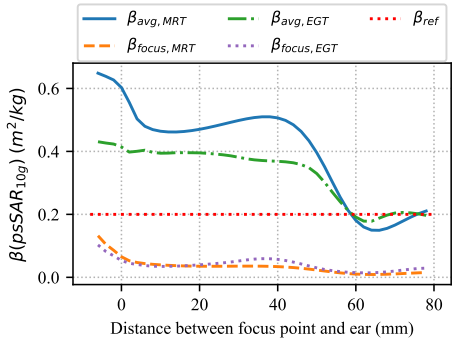

(b)

Fig. 5. (a) SAR_{ear} (b) $psSAR_{10g}$ normalized to the incident power density as a function of distance between the focus point and ear of the Ella phantom using MRT (β_{MRT}) and EGT (β_{EGT}). β_{avg} indicates normalization with the average S_{inc} and β_{focus} indicates normalization with the S_{inc} at the focus point. β_{ref} is the reference value calculated using the basic restrictions set by ICNIRP.

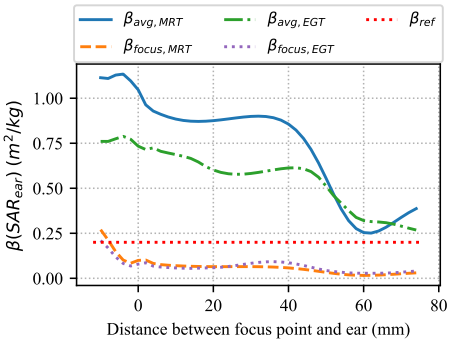

(a)

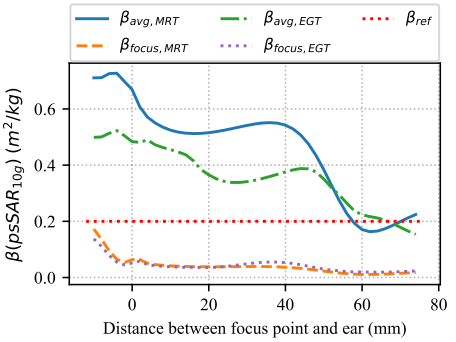

(b)

Fig. 6. (a) SAR_{ear} (b) $psSAR_{10g}$ normalized to the incident power density as a function of distance between the focus point and ear of the Duke phantom using MRT (β_{MRT}) and EGT (β_{EGT}). β_{avg} indicates normalization with the average S_{inc} and β_{focus} indicates normalization with the S_{inc} at the focus point. β_{ref} is the reference value calculated using the basic restrictions set by ICNIRP.

quantities were determined using two different strategies and compared with the ICNIRP guidelines. Normalizing to the average incident power density almost always results in a violation of the guidelines, while normalizing to the incident power density almost always complies with the guidelines. This last normalization also directly scales with the power density needed by the UE.

The same approach can be used for focusing at other locations, e.g., UE in front of the eyes, as well as for the higher frequencies, i.e., millimeter-waves, that are expected to be used in 5G networks. Future work consists of studying other locations of UE and therefore other focusing locations, higher frequencies, and other phantoms.

Acknowledgment

This research was funded by the ETAIN project. The ETAIN project is funded by the European Union's Horizon Europe research and innovation funding programme under grant agreement No. 101057216. Arno Thielens is a postdoctoral fellow of the Research Foundation Flanders (FWO) under grant agreement No. 1283921N.

References

[1] I. Liorni *et al.*, "Evaluation of Specific Absorption Rate in the Far-Field, Near-to-Far Field and Near-Field Regions for Integrative Radiofrequency Exposure Assessment," *Radiation Protection Dosimetry*, vol. 190, no. 4, pp. 459–472, 09 2020.

[2] T. L. Marzetta, "Noncooperative Cellular Wireless with Unlimited Numbers of Base Station Antennas," *IEEE Transactions on Wireless Communications*, vol. 9, no. 11, pp. 3590–3600, 2010.

[3] M. Velghe, S. Aerts, L. Martens, W. Joseph, and A. Thielens, "Protocol for personal RF-EMF exposure measurement studies in 5th generation telecommunication networks," *Environmental Health*, vol. 20, no. 1, pp. 1–10, 2021.

[4] M.-C. Gosselin *et al.*, "Development of a new generation of high-resolution anatomical models for medical device evaluation: the Virtual Population 3.0," *Physics in Medicine & Biology*, vol. 59, no. 18, p. 5287, 2014.

[5] P. Hasgall *et al.*, "IT'IS Database for thermal and electromagnetic parameters of biological tissues, Version 4.0," *IT'IS*, 2018.

[6] S. Shikhantsov *et al.*, "Massive MIMO Propagation Modeling With User-Induced Coupling Effects Using Ray-Tracing and FDTD," *IEEE Journal on Selected Areas in Communications*, vol. 38, no. 9, pp. 1955–1963, 2020.

[7] S. Saunders and A. Aragón-Zavala, *Antennas and Propagation for Wireless Communication Systems*. Wiley, 2007.

[8] International Commission on Non-Ionizing Radiation Protection, "Guidelines for limiting exposure to electromagnetic fields (100 kHz to 300 GHz)," *Health Phys.*, vol. 118, no. 5, pp. 483–524, 2020.